ELSEVIER

Journal of Alloys and Compounds 347 (2002) 105–109

Journal of ALLOYS AND COMPOUNDS

www.elsevier.com/locate/jallcom

X-ray diffraction and scanning electron microscopic characterization of electrolytically hydrogenated nickel and palladium

S.S.M. Tavares[a,b,*], S. Miraglia[a], D. Fruchart[a], D.S. dos Santos[c]

[a]*Laboratoire de Cristallographie, CNRS BP 166, 38042 Grenoble Cedex 9, France*

[b]*Depto. de Engenharia Mecânica, UFF, R. Passo da Pátria, 156, CEP 24210-240, Niterói, Brazil*

[c]*Departamento de Engenharia Metalúrgica e de Materiais/COPPE/UFRJ, C.P. 68505, CEP 21945-970, Rio de Janeiro, Brazil*

Received 25 March 2002; received in revised form 17 April 2002; accepted 17 April 2002

Abstract

The effects of hydrogen insertion by electrolytic charging in H_2SO_4 solution in pure nickel and palladium were investigated. The hydrogenated phases of Ni and Pd and their stability during aging were determined by X-ray diffraction. The $NiH_{0,68}$ hydride and the α-Ni phase were distinguished by scanning electron microscopy (SEM) operating in the backscattered electrons mode. Interesting features about the intergranular cracks developed during and after charging are discussed.

Keywords: Hydrogen absorbing materials; Electrochemical reactions; X-ray diffraction; Microstructure; SEM

1. Introduction

The physical and mechanical properties of many transition metals undergo drastic changes when hydrogen is introduced in the metal lattice. Here we have concentrated on the Pd–H and Ni–H systems. As these two systems show some similarities, they were many times studied together [1–3]. In the case of nickel, the hydrogenation by gaseous or electrochemical method leads to the formation of the hydride $NiH_{0.7}$ (phase β). The phase α-Ni dissolves only 0.03%at.H [4] and is ferromagnetic, while the $NiH_{0.7}$ is reported to be paramagnetic [4–6] or to present weak ferromagnetism [7]. In the case of palladium, two hydrogenated phases are previewed in the phase diagram at 1 atm [8]: α, which dissolves 8%at.H (H/Pd≈0.09) at room temperature and β, which can dissolve from 34% to 42%at.H (H/Pd from ~0.51 to ~0.72). The β-$NiH_{0.7}$ hydride is reported to be very unstable at room temperature and normal pressure [9], while the hydrogenated palladium phases are more stable under the same conditions. In all these mentioned phases the hydrogen atoms occupy the octahedral interstices.

Other hydrogenated phases may be produced in both systems by high pressure hydrogenation. Hanson et al. [4] obtained an atomic ratio H/Ni=1 applying a hydrogen pressure of 1.5 GPa. Fukai [10] and dos Santos et al. [11] obtained the phases PdH and $PdHVacH_4$ in high pressure experiments. Oates [12] have commented on the results obtained by Fukai [10] and inferred that an atomic ratio H/Pd≈1.2 must have been reached in their experiments. Atomic ratios (H/Pd and H/Ni) equal to or higher than one are rather difficult to obtain by electrolytic methods. Brand et al. [13] have obtained a very unstable phase with H/Pd>1.2 by electrolytic charging at 195 K and cooling to 120 K just after the hydrogenation.

In the present work thin foils of palladium and nickel were hydrogenated by electrolytic charging. The materials were then characterized by X-ray diffraction and scanning electron microscopy (SEM). The results show interesting features about the surface aspect, the hydrogenated phases produced and their stability during aging. The behaviour of the two metals under hydrogenation are compared and discussed.

2. Experimental

Thin foils of nickel and palladium were hydrogenated by electrolytic charging in a 1 N H_2SO_4 solution with a current density in the 15–25 mA/cm^2 range. As_2O_3 was

*Corresponding author.
E-mail address: ssmtavares@ig.com.br (S.S.M. Tavares).

0925-8388/02/$ – see front matter
PII: S0925-8388(02)00674-6

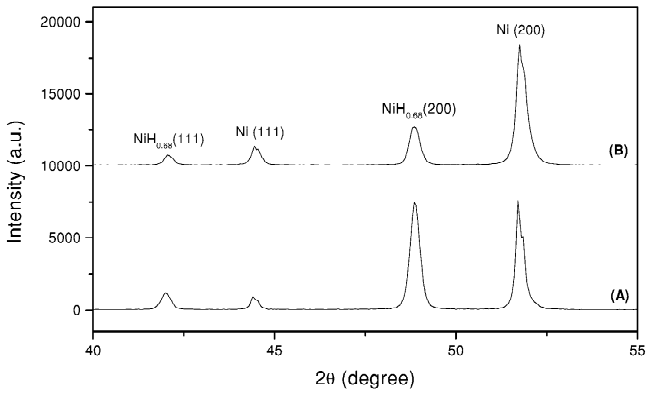

Fig. 1. Diffractogram of thin foils of nickel: (a) before and (b) just after the hydrogenation.

used as catalyst in a concentration of 5×10^{-5} mol/l. Nickel was charged for 24 h and palladium for 5 h. The hydrogenated samples were analysed by X-ray diffraction and scanning electron microscopy immediately after charging and after desorption. The nickel samples were aged for several hours at room temperature and palladium was naturally aged for some days and also heat treated at 100, 200 and 400 °C for hydrogen desorption.

X-ray diffraction was carried out in a SIEMES D-5000 diffractometer with KαCu radiation. SEM images were obtained in a JEOL 840A microscope.

3. Results

3.1. Phases formed during hydrogenation

Fig. 1 shows the X-ray diffractogram of the hydrogenated nickel immediately (curve a) and 4 h after charging (curve b). The electrolytic hydrogenation

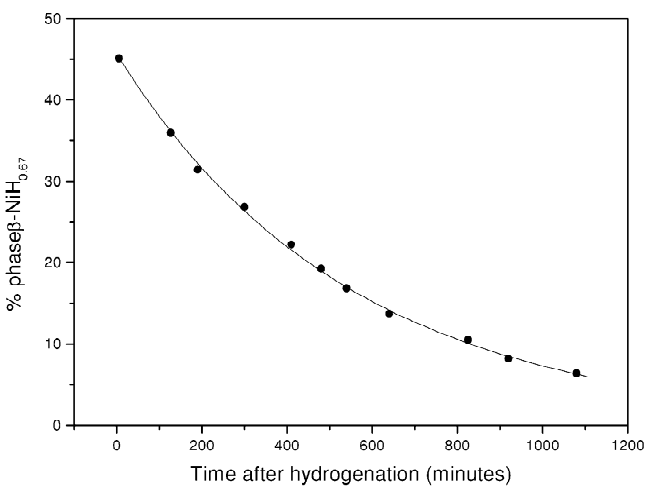

Fig. 2. Amount of nickel hydride as a function of time after hydrogenation.

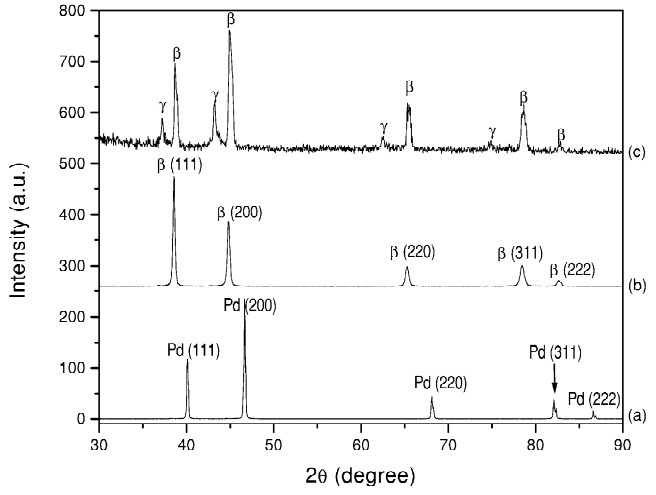

Fig. 3. Diffractograms of palladium: (a) before hydrogenation, (b) after hydrogenation with As_2O_3 and (c) without As_2O_3.

produces the metastable hydride $NiH_{0.67}$ with lattice parameter 3.71 Å. Fig. 2 describes the kinetics of $NiH_{0.67}$ decomposition determined by X-ray diffraction.

Fig. 3 shows the X-ray diffractogram of pure palladium (curve a), palladium hydrogenated with (curve b) and without As_2O_3 (curve b). In the samples hydrogenated without catalyst all of the palladium was transformed into β-$PdH_{0.63}$. The As_2O_3 addition to the electrolyte increases the hydrogen fugacity and, as a result, a highly hydrogenated phase very similar to that obtained by Brand et al. [13] appears together with the β-$PdH_{0.63}$ hydride. This phase (here denoted by γ) can be indexed as an f.c.c. phase with lattice parameter roughly equal to $a=4.20$ Å. Considering the volume occupied by a hydrogen atom as 2.8 $Å^3$ [14] this phase should have an H/Pd ratio equal to 1.36, which means that all octahedral and also some tetrahedral interstitial sites are occupied by hydrogen atoms.

The hydrogenated phases of palladium are more stable than the nickel hydride. In the first 24 h of natural aging the X-ray diffraction pattern did not change. However, after aging for 120 h, an intermediate hydride can be clearly seen in Fig. 4. Considering the two reflections indicated by arrows the lattice parameter of this hydride is 3.984 Å, which corresponds to a ratio H/Pd≈0.39. The palladium phase appeared only after 240 h of natural aging (Fig. 4).

Fig. 5 shows the X-ray patterns of palladium hydrogenated and subsequently heat-treated at 100 °C, 200 °C and 400 °C (1 h for each temperature). The phases α, γ-PdH_x and β-PdH_x ($a\approx4.01$, $x=H/Pd\approx0.50$) are present after the heat treatment at 100 °C. The lattice parameter of the phase α-Pd is 3.869 Å, which is smaller than that of the original foil (3.890 Å). Some authors [10,11] have correlated the lattice parameter contraction observed in nickel and palladium to the hydrogen induced vacancy production. If we employ the same methodology used by

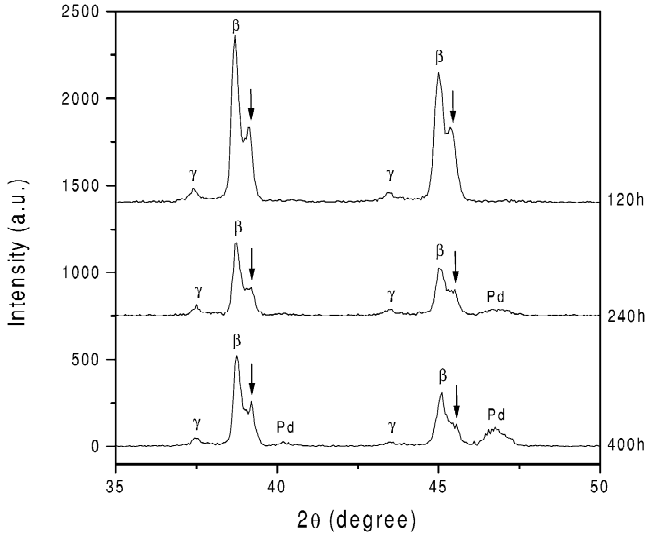

Fig. 4. Diffractograms of hydrogenated palladium after 120, 240 and 400 h.

Fukai [10], with a vacancy relaxation volume $v_r = -0.29$, the resultant vacancy concentration would be about 6%.

The diffractograms obtained after heat treatments at 200 °C and 400 °C show the phase α-Pd with $a = 3.880$ Å and an hydrogenated phase, here denoted by β′, with $a = 4.047$ Å (H/Pd≈0.66). This lattice parameter is located between that of the phases β and γ. It is possible that these two phases have formed another phase with an intermediate hydrogen content.

3.2. SEM analysis

SEM analysis with hydrogenated nickel presents two interesting features. First, the two phases, α-Ni and β-$NiH_{0.67}$, could be distinguished in the backscattered electrons mode, due to the difference in densities ($\rho_{Ni} = 8.91$ g/cm^3, $\rho_\beta \approx 7.66$ g/cm^3) or average atomic number ($Z_{Ni} = 28$ and $Z_\beta \approx 17$). Fig. 6 show the hydrogenated foil immediately after hydrogenation. The α-Ni phase is the bright one, concentrated at the grain boundaries. After 4 h, the same sample is shown in Fig. 7. The decrease of the hydride phase (dark regions) observed by X-ray diffraction is also observed when comparing Figs. 6 and 7. The second interesting feature concerns the intergranular cracks

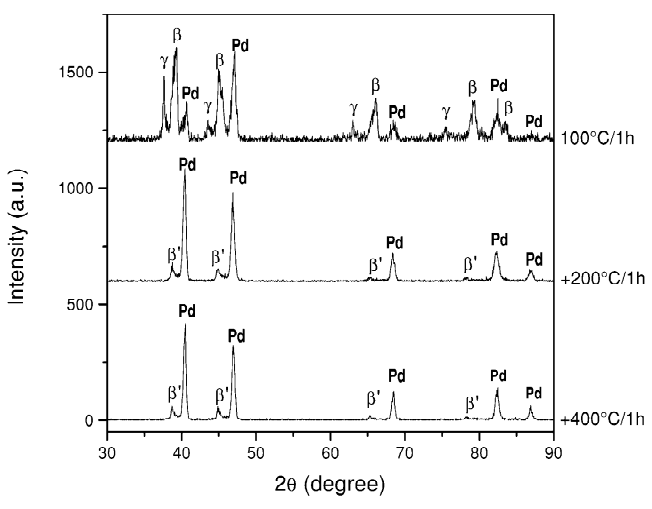

Fig. 5. Diffractograms of hydrogenated palladium aged at 100, 200 and 400 °C.

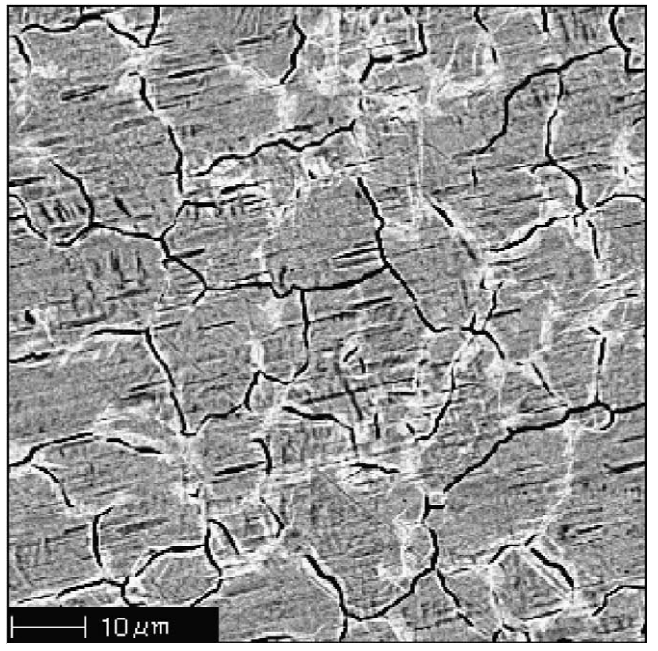

Fig. 6. Backscattered electron image of nickel obtained just after hydrogenation.

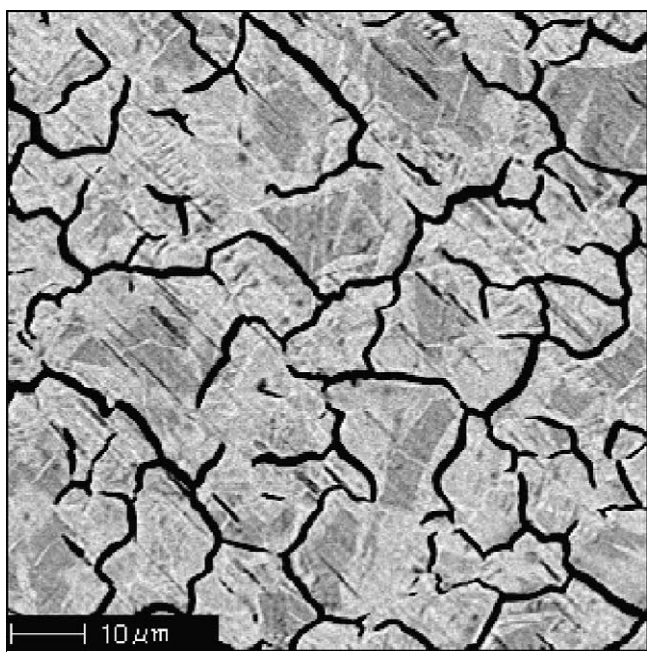

Fig. 7. Backscattered electron image of nickel obtained 4 h after hydrogenation.

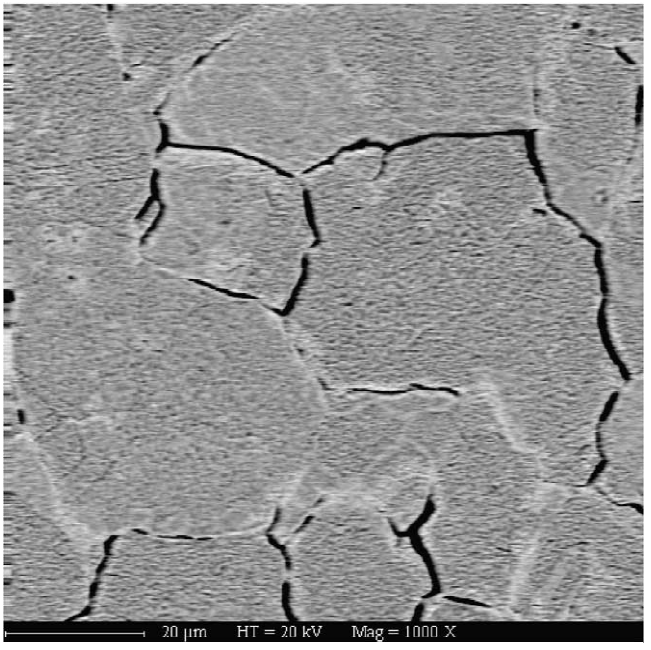

Fig. 8. Backscattered electron image of nickel obtained just after hydrogenation.

created during the electrolytic charging, which can be attributed to the high susceptibility of nickel to hydrogen embrittlement [15] and to the development of contraction and tensile stresses during the hydrogen absorption and desorption, respectively [16]. Figs. 6 and 7 suggest that the α-Ni phase grows from the grain boundaries which are preferential sites for the hydrogen desorption, specially when the cracks are created.

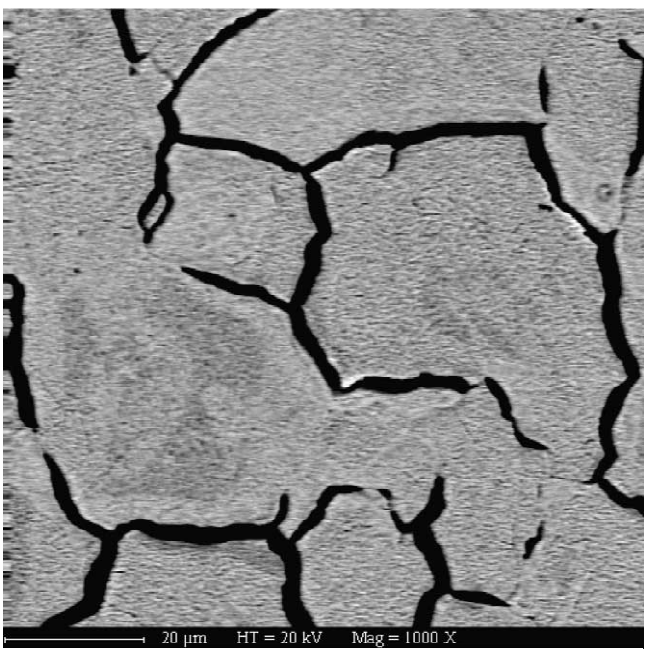

Fig. 9. Backscattered electron image of nickel obtained 18 h after hydrogenation (same region of Fig. 8).

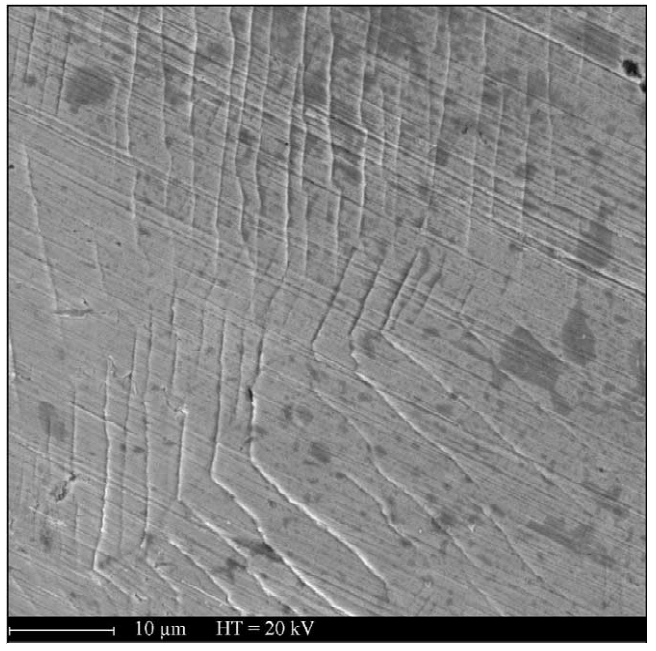

Fig. 10. Slip bands produced in hydrogenated palladium foil.

During the natural aging, the nickel hydride decomposition is accompanied by lattice contraction that promotes mainly tensile stresses. These stresses concentrate in the pre-existing cracks and causes the latter to open. This explains the increase of the average crack thickness that can be observed when comparing Figs. 6 and 7. The crack propagation during natural aging can still better be observed by following the evolution in the same region (see Figs. 8 and 9).

Previous works [17,18] have shown the presence of solid solution hardening effect of hydrogen in palladium. However, although it is much more easily hydrogenated, the palladium is much less susceptible to hydrogen embrittlement than nickel. Only slip bands are observed after electrolytic charging (Fig. 10). It should also be pointed out that, as the palladium hydride phases are quite stable, decomposition does not occur during the hydrogenation, which means that only compressive stresses are developed. In the case of nickel, as the hydride is very unstable at room temperature, decomposition also occurs during the charging and this induces the tensile stresses.

When the palladium foil is heat treated at 400 °C for hydrogen desorption, tensile stresses are developed [19]. These stresses may thus induce intergranular microcracks, as shown in Fig. 11.

4. Conclusions

The nickel hydride $NiH_{0.67}$ produced by electrolytic charging and the α-Ni phase can be distinguished by SEM in the backscattered mode. The nickel foils present many

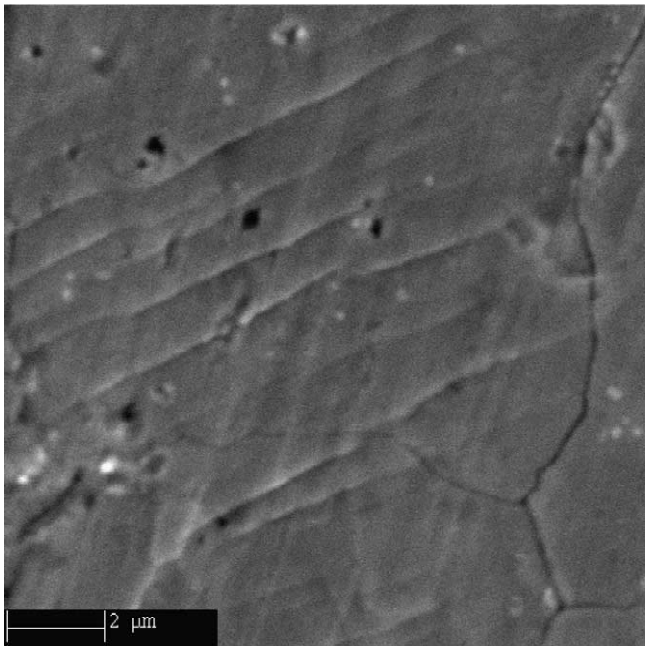

Fig. 11. Slip bands and intergranular microcrack in palladium foil aged at 400 °C after hydrogenation.

intergranular cracks just after the hydrogenation, and these cracks become larger and propagate during room temperature aging for some hours, which is attributed to tensile stresses developed during hydride decomposition.

In palladium, two hydrogenated phases (β-$PdH_{0.63}$ and γ-$PdH_{1.36}$) can be produced by electrolytic charging in 1 N H_2SO_4 solution with As_2O_3 addition. These phases are very stable at room temperature, and it is only after 120 h that the desorption starts. During aging treatment the phase γ-$PdH_{1.36}$ exists till 100 °C. After that, in the aging at 200 °C and 400 °C a hydrogenated phase with $H/Pd = 0.66$ is still observed together with the α-Pd phase. Palladium is much less susceptible to hydrogen embrittlement. Nevertheless, small intergranular cracks may be formed during hydrogen desorption with temperature, as a consequence of the tensile stresses developed.

Acknowledgements

S.S.M. Tavares would like to acknowledge CNPq (Brazilian National Research Agency) for financial support (470385/01-4 NV).

References

[1] O.B. Christinsen, P. Stoltze, K.W. Jacobsen, J.K. Norskov, Phys. Rev. B 41 (18) (1990) 12413–12423.
[2] J.B. Kepka, E.W. Czaputowicz, Phys. Rev. B 19(4) (1979).
[3] Yurechev, E.G. Ponyatovskii, Phys. Stat. Sol. A 58 (1980) 57.
[4] M. Hanson, H.J. Bauer, J. Alloys Comp. 179 (1992) 339–349.
[5] H.J. Bauer, B. Baranowskii, Phys. Stat. Sol. A 40 (1977) K35.
[6] G.K. Wertheim, D.N.E. Buchanan, J. Phys. Chem. Solids 28 (1967) 225–230.
[7] R. Wisniewski, A.J. Rostocki, Phys. Rev. B 4 (12) (1971) 4330–4332.
[8] ASM Metals Handbook, Vol. 8, 8th Edition, ASM, 1973.
[9] G.K. Wertheim, D.N.E. Buchanan, J. Phys. Chem. Solids 28 (1967) 225.
[10] Y. Fukai, Phys. Rev. Lett. 73 (12) (1994) 1640.
[11] D.S. dos Santos, D. Fruchart, S. Miraglia, J. Alloys Comp. 291 (1999) L1.
[12] W.A. Oates, H. Wenzl, Scripta Metall. Mater. 33 (2) (1995) 185.
[13] R.A. Brand, H. Georges, L. Lelaurain, J. Phys. F 10 (1980) L257.
[14] N. Tsukuda, K. Itoh, N. Morioka, H. Ohkubo, E. Kuramoto, J. Alloys Comp. 293–295 (1999) 174.
[15] J. Yao, S.A. Meguid, J.R. Cahoon, Met. Trans. A 24A (1993) 105.
[16] T. Zakrocdzymski, Z. Szklarska-Smialowska, M. Smialowski, Corrosion 39 (6) (1983) 207.
[17] R.J. Smith, D.A. Otterson, J. Less Common Met. 24 (1971) 419.
[18] C. Anderton, N. Strother, J. Pote, R. Foley, K. Rebeiz, S. Nesbit, A. Craft, Scripta Mater. 35 (8) (1996) 1013.
[19] S.Y. Liu, Y.H. Kao, Y. Oliver Lu, T.P. Peing, J. Alloys Comp. 316 (2001) 280.